Journal of Engineering Science and Technology
Vol. 18, No. 2 (2023) 1137 - 1152

RECONFIGURABLE COMPOSITE RIGHT/LEFT-HANDED TRANSMISSION LINE ANTENNA BASED MINKOWSKI- STEPPED IMPEDANCE RESONATOR STRUCTURE FOR 5G COMMUNICATION NETWORKS

MARWA M. ISMAIL[1,*], TAHA A. ELWI[2], A. J. SALIM[1]

[1]Electrical Engineering Department, University of Technology, Baghdad, Iraq
[2]Communication Engineering Department, Al-Ma'moon University College, Baghdad, Iraq
*Corresponding Author: eee.19.06@grad.uotechnology.edu.iq

Abstract

This paper presents a design of a metamaterial antenna based on a Composite Right/Left-Handed Transmission Line (CRLH-TL). The proposed antenna is constructed from 17 unit cells of CRLH-TL with an Electromagnetic Band Gap (EBG) of the 1st order Minkowski- Stepped Impedance Resonator (SIR). The antenna is printed on a Taconic RF-43 substrate with thickness=1.57 mm and with an overall size of 204.6 * 40 mm^2. The CRLH and fractal structure achieve frequency reconfigurable, compactness, multiple- bands, and high radiation performance. 17 PIN diodes are used to control the antenna performance and show its frequency reconfiguration; 6 cases are selected among 217 cases due to space limitations. As a result, the antenna design can operate in various wireless bands such as Radars [4.2-4.3 GHz and 4.6-4.9 GHz], Wi-Max [5.8 GHz], Wi-Fi [4.9 GHz, 5 -5.8 GHz], and 5G sub-6-GHz [4.6 GHz and 5-5.9 GHz], which indicates the novelty of the proposed antenna and the possibility of using it in various applications. Computer Simulation Technology- Microwave Studio (CST-MWS) is used to design and simulate the proposed antenna. The Minkowski –SIR antenna achieved dual-band operation with maximum gain equal to 12.4 dBi and 10.8 dBi at 4.89 GHz and 5.4 GHz, respectively.

Keywords: 5G Communication, CRLH-MTM, Frequency reconfigurable, Minkowski Curve, Stepped impedance resonator.

1. Introduction

With each decade, the population increases, and the need to provide the necessary communication requirements increases; thus, communication systems have to offer small antennas, low cost, and high performance to keep up with this rapid increase [1-3]. Therefore, several methods of designing miniature antennas by loading metamaterials have recently emerged [4].

The Metamaterials (MTM) are designed and fabricated using a resonance approach or transmission lines. Transmission lines have structures with negative constitutive parameters, while Split-Ring Resonators (SRR) and Complementary Split-Ring Resonators (CSRR) represent the resonant approach [5]. Zero-order resonance is an important feature that distinguishes transmission lines, as the antenna resonance becomes specific and independent of transmission line length [6]. However, compact design and use of via in the MTM-structures have resulted in antennas with narrow bandwidth, low efficiency, and low gain [7], and highly complex designs due to via that cause losses in most wireless applications to their high cost [8, 9].

To improve antenna performance and overcome the problems mentioned above. MTM has been included in the antenna structure design using various methods [10], such as Electromagnetic Band Gap (EBG), Perfect Electric Conductor (PEC), Artificial Magnetic Conductor (AMC) reflector, and MTM- substrate loadings. On the other hand, these multi-layer antennas suffer from many drawbacks, such as narrow bandwidth, low gain, low efficiency [11], and the presence of via, which complicates the antenna manufacturing process [12]. Therefore, these antennas are not suitable for applications that require highly efficient antennas with less complex designs. The following are some of the work processes in this field.

The pattern and frequency reconfiguration are achieved using 4 PIN diodes, and the antenna can operate at three bands with good gain [13]. A dual wideband pattern reconfigurable antenna was proposed for wireless networks; omnidirectional radiation patterns are achieved at 2.4 GHz and directional radiation patterns at 5.8 GHz with good gain and S_{11} [14]. Ismail et al. [15] proposed an EBG structure for a dual-band pattern reconfigurable antenna. The antenna operates at 2.45 GHz and 5.8 GHz with good gain. In addition, it can shift the beam at three angles 0°, +26°, and −26°. 8 PIN diodes are used for frequency and pattern reconfiguration [16]; the proposed antenna operates at various bands (2.6 GHz, 3.5 GHz, 4.2 GHz, 4.5 GHz, and 5 GHz) with beam steer capability. Reji and Manimegalai [17] presented a V-shaped frequency reconfigurable antenna 2 PIN diodes in the ground plane are used for reconfiguration, and a peak gain of 6dBi at 5.3GHz is achieved. Prakash et al. [18] proposed a reconfigurable pattern antenna with a PIN switching network; four beams are achieved with a gain between 2.9 to 4.33 dBi among the operated beams. Anantha et al. [19] proposed a polarization reconfigurable antenna array. 16 PIN diodes are used for polarization reconfiguration for the 5.7–6.0 GHz operating band.

In this research, the MTM- antenna is introduced with a new structure to achieve high gain and efficiency across the operating bands. The proposed design consists of an asymmetric T-shaped CRLH unit cell loaded with Minkowski -Stepped Impedance Resonator SIR structure etched on the backside of the substrate and fed with an asymmetric coplanar waveguide feed structure. As a result, the proposed antenna achieved a dual-band operation with a maximum gain of 12.4 dBi and 10.8 dBi at 4.8 and 5.4 GHz, respectively.

This paper is organized as follows: - First, the Minkowski - SIR antenna design and its geometrical details are discussed in Section 2. Next, the parametric study is discussed in Section 3, where a detailed analysis shows the effect of parameters on antenna performance. Next, frequency reconfiguration is discussed in Section 4, and a comparison to the latest research is discussed in Section 5, followed by the conclusion in Section 6.

2. Antenna Design Based On Minkowski - SIR Structure

Figure 1 shows the CRLH antenna structure; the unit cell consists of an interdigital capacitor C_{IDC} combined with stub inductor L_{TS} [20]. Such a combination creates the Left-Handed LH branch, while the parasitic effects create the Right Handed RH branch, limiting the antenna performance [21]. A 1st order Minkowski structure curve with SIR was etched on the substrate's back surface to amplify the magnetic field's effect, which increases the displacement current flow in the direction of the unit cell and thus enhances the antenna performance. The asymmetric CPW feeding technique was used to feed the CRLH unit cell, as the ground dimensions are different on both sides of the feeding structure. A half-circle matching network is introduced to suppress the back wave radiation. The CRLH-TL is printed on Taconic RF-43 substrate with relative permittivity ε_r= 4.3, permeability μ_r=1, thickness= 1.57mm, and loss tangent $\tan_\delta$ = 0.003; it is used for their characteristics represented by low loss in comparison to FR-4 substrate, in addition, their stable Dielectric Constant (DK) over temperature and frequency changes The proposed CRLH structure is presented in Fig. 1 where the top- back view details are given and explained. Fig. 1(a) showed the top view of the proposed antenna where 17 CRLH unit cells are connected in series and coupled to 17 EBG inclusions of 1st order Minkowski -SIR structure as shown in Fig. 1(b); A half circle matching network was used to increase the impedance matching as shown in Fig. 1(c). the proposed antenna was attached to a rectangular pad, see Fig. 1(d), through a PIN diode to control the antenna performance by changing the state value through varying bias voltage. These variations affect the harmonic fluctuations of the plasmonic surface current on metamaterial structure [22]; as a result, the resonance frequency can be changed to produce multiple bands suitable for various wireless applications. Finally, a matching impedance was added at the end of the antenna to reduce reradiated power and increase impedance matching. Subsequent sections provide more details about other antenna parts.

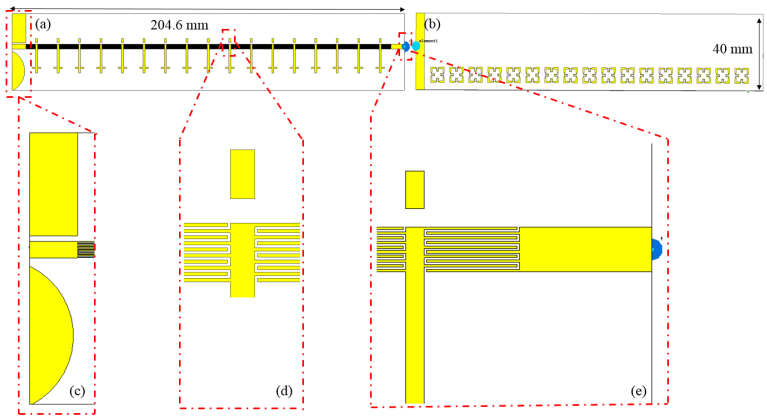

Fig. 1. Geometrical antenna structure (a) top-view (b) back-view (c) coplanar waveguide feeding structure (d) rectangular pad (e) matching impedance.

2.1. CRLH-MTM geometrical details

The CRLH unit cell consists of a left-handed component represented by an inter-digital capacitor and T-stub inductor; see Fig. 2. The inter-digital capacitor contains five fingers on each side, representing the series capacitance, and the T-stub inductor represents the shunt inductance. A Minkowski-SIR structure was used to replace via and reduce its effects. The ground plane stores energy, representing an interactive (capacitive effect) [23]; therefore, a 1st order Minkowski-SIR inclusion is etched on the back surface of the substrate to reduce the tripped energy within the ground plane with minimum conduction loss; thus reducing antenna loss and equalizing the capacitive impact. However, the 1st order Minkowski-SIR structure and the substrate generated the parasitic effects for the right-handed branch, limiting the antenna gain-bandwidth product.

In addition, the ground plane represents a reflector that reflects the propagating wave [24], with a phase opposite to the source wave phase, where the source wave represents the wave that propagates along with the radiator; thus, destructive interference occurs, which cancel out or significantly limits the source wave and the radiation efficiency. As a result, the gain decreases due to field cancellation [25]. In the proposed design, the Minkowski-SIR unit cells replaced the ground layer, and thus the losses caused by the ground plane were significantly reduced.

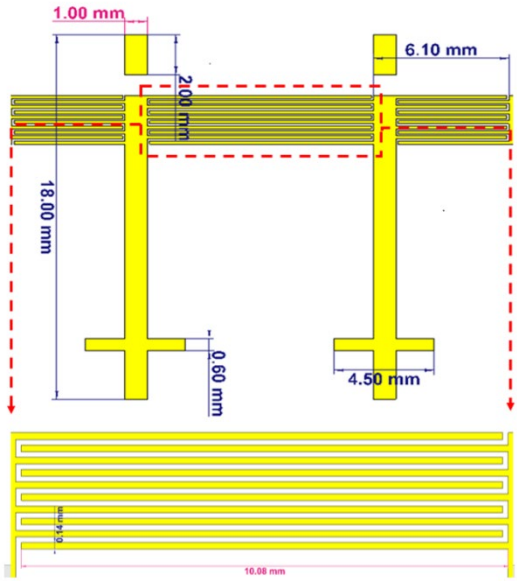

Fig. 2. CRLH dimensions.

2.2. EBG Structure geometrical details

EBG at high and microwave frequencies are periodic or quasi-periodic structures caused by metallic impurities in dielectric or magnetic material [26]. EBG structures have been used in many applications due to their distinctive properties to reduce surface waves and enhance overall performance [27]. In this design, an array of 17×1 1st order Minkowski-SIR unit cells is etched from the back surface of the substrate and fill an area equal to (8.02×8.02) mm^2, as shown in Fig. 3.

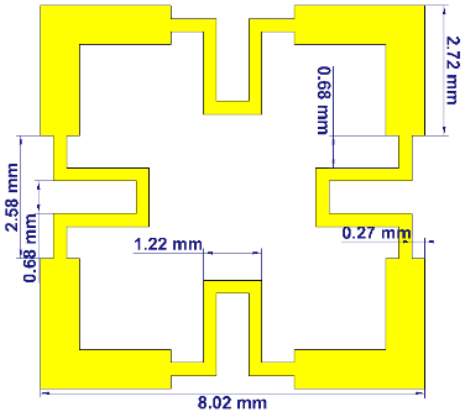

Fig. 3. Minkowski-SIR curve dimension.

This array type generates a capacitive gap between neighbouring cells, which can be expressed by Eq. (1) [28].

$$c = \frac{p\varepsilon_o(1+\varepsilon_r)}{\pi} cosh^{-1}(\frac{p+g}{g}) \quad (1)$$

The EBG structure allows high frequencies to pass through and prevents low frequencies by acting as a high pass filter, showing its capacitive behaviour [29]. The capacitive effect is equal on both sides of the unit cell, and this returns to the fact that the cell is balanced according to the stub –length; thus, the effect of capacitive reactance between neighbouring cells has an equal impact on suppressing surface currents, which is given by Eq. (2).

$$xc = \frac{1}{2\pi f c_{gap}} \quad (2)$$

3. Parametric Study

This section presents a detailed explanation of the antenna design process and the basic parameters that played an important role in arriving at the final results. The results were analysed using a CST software tool based on a finite integration technique (FIT) for microwave devices [30]. A time domain solver was selected for wideband or multiband antennas. All the dimensions are in (mm), the Minimum frequency is 0GHz, and the maximum frequency is 6 GHz; a single layer is used for the proposed design. It is found from the proposed study that gain-bandwidth enhancement is achieved due to eliminating via conduction losses, ground plane capacitive losses, and surface wave suppression by the proposed EBG defects. The simulation and analysis process are divided into the following parts:-

3.1. C_{IDC} effect

The effect of C_{IDC} fingers on the antenna performance was studied and explained. The C_{IDC} fingers were changed from 1 to 5, and a detailed study was conducted to calculate the realized gain and S_{11} in each case. By increasing the number of fingers, the matching impedance is increased due to eliminating the storing losses by equalizing the capacitive reactance to the inductive reactance within the circuit.

However, the increase in the number of fingers does not affect the antenna gain because the electric field gradient on the surface of the miniaturized -unit cell is minimal and insignificant, as shown in Fig. 4.

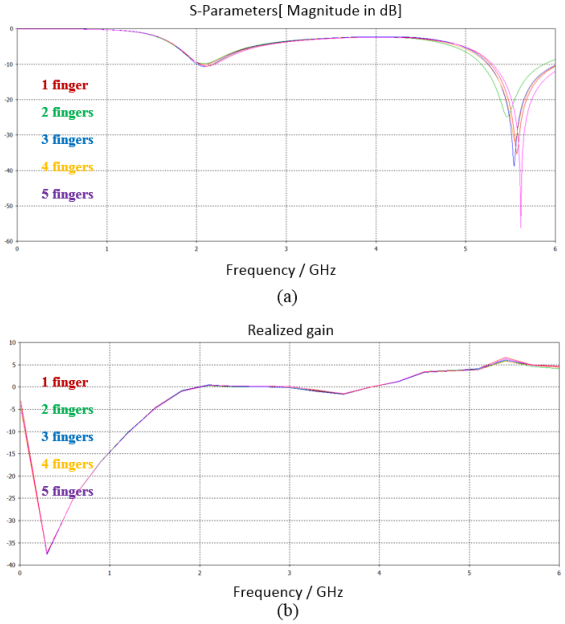

Fig. 4. C_{IDC} parametric study (a) S_{11} (b) realized gain.

3.2. L_{TS} effect

The inductor length was changed from 12 to 18 mm, and the realized gain and S_{11} were calculated in each case. Increasing the length of the inductor from 12 to 18 mm; acts as a capacitive tuner by equalizing the capacitive effect to the inductive effect, which reduces storage losses within the antenna and increases radiation efficiency, increasing the antenna gain. As a result, the realized gain rises from 6.69 to 8.8 dBi at 5.4 GHz. At the end of the inductor, the T-shaped component acts as a small patch that allows a high-energy field distribution and thus increases the gain to reach a maximum value of 9.5 dBi for the 2-CRLH unit cell. It is good to mention that the antenna has no resonance for frequencies lower than 2 GHz, as the realized gain starts to arise after 2 GHz. see Fig. 5.

3.3. CRLH unit cell

The CRLH unit cell can be fragmented into four parts; each represents a model. For example, model 1 represents transmission line T_L only; model 2 combines T_L to the C_{IDC} with five fingers on each side; model 3 represents [T_L+ C_{IDC} + L_{TS}], where the inductor acts like a capacitive tuner, and model 4 represents the CRLH unit cell with a Minkowski-SIR inclusion as shown in Fig. 6. S_{11} and realized gain are calculated for each model and illustrated in Fig. 7; a significant decrease in the proposed cell size is observed after introducing the Minkowski - SIR curve by shifting the 2nd frequency mode from 5.5GHz to 2.9GHz. With the gain remaining unchanged. Finally, a flowchart illustrating the design process and the influence factors is given in Fig. 8.

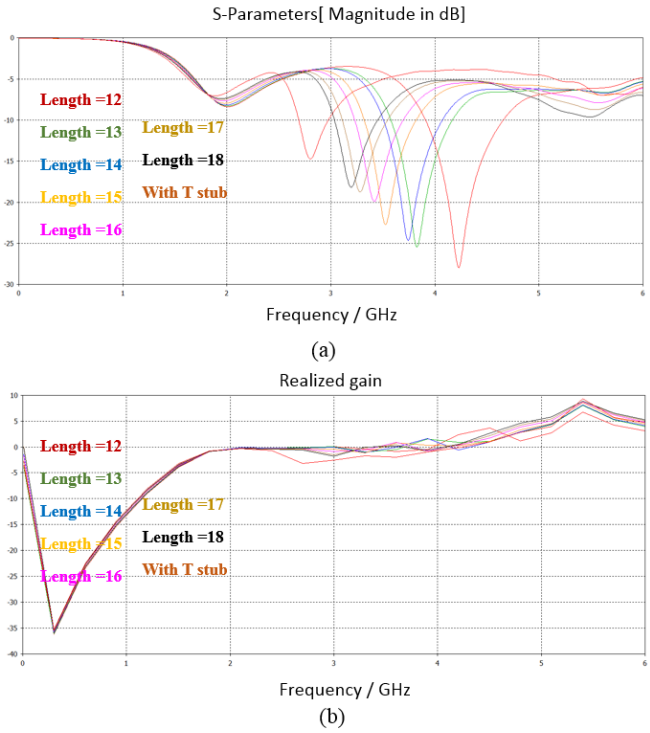

Fig. 5. T-stub inductor parametric study (a) S_{11} (b) realized gain.

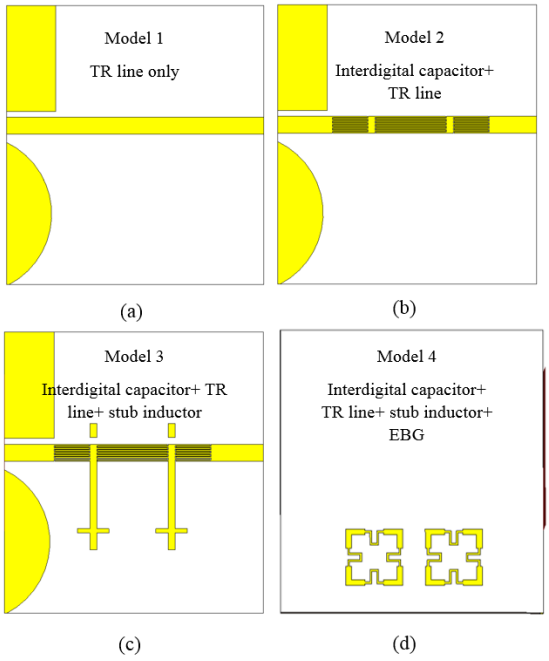

Fig. 6. CRLH-unit cell structure (a) Model1 (b) Model 2(c) Model 3 and (4) Model 4.

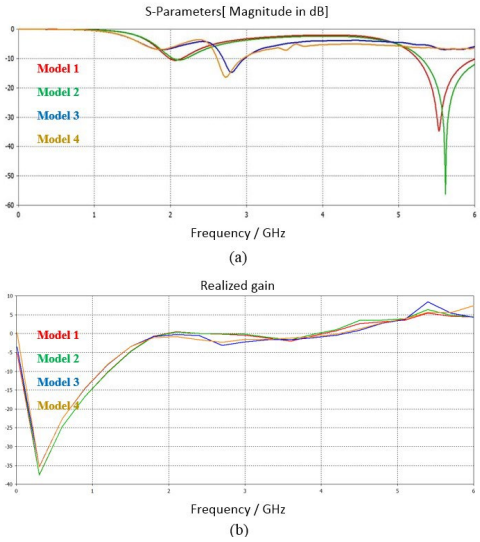

Fig. 7. CRLH-unit cell parametric study (a) S_{11} (b) realized gain.

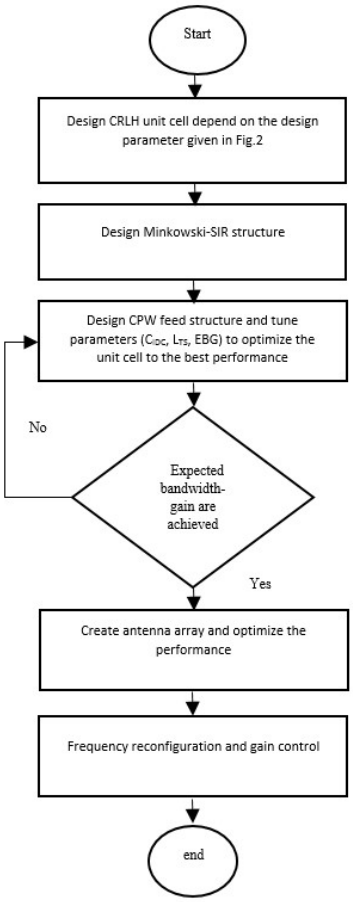

Fig. 8. The design procedure.

3.4. Antenna array with and without EBG defects

The EBG structure results from constructing Minkowski fractal topology with the SIR technique on a traditional square ring resonator. The proposed EBG structure is inspired by Ziboon and Ali [31] to obtain a dual band using a single resonator. This EBG defect was constructed in two steps; first, the SIR technique was added to all sides of the square loop resonator. Next, 1st-order Minkowski fractal curves were applied to generate the proposed EBG defects.

This section studies the impact of EBG defects on the array's performance. Two cases were taken, the first with EBG defects and the second with no EBG defects; the radiation pattern and S_{11} were measured in each case. The frequency was shifted with EBG defects with higher impedance matching, resulting in a better gain. The gain reached the highest value at 4.89 GHz with 12.4 dBi and 10.8 dBi at 5.4 GHz; the EBG structure reduces the surface waves resulting in better gain and S_{11}, as shown in Fig. 9. The equivalent circuit model using ADS software is given in Fig. 10 with S_{11}.

When the antenna is bent under deformation, Theoretically, the effective length will decrease and continue to decrease with the increase in the bending; therefore, a resonance frequency will shift, reducing the overall performance. But as long as the radiating element doesn't affect by bending, the antenna still operates with a good performance in the operating range.

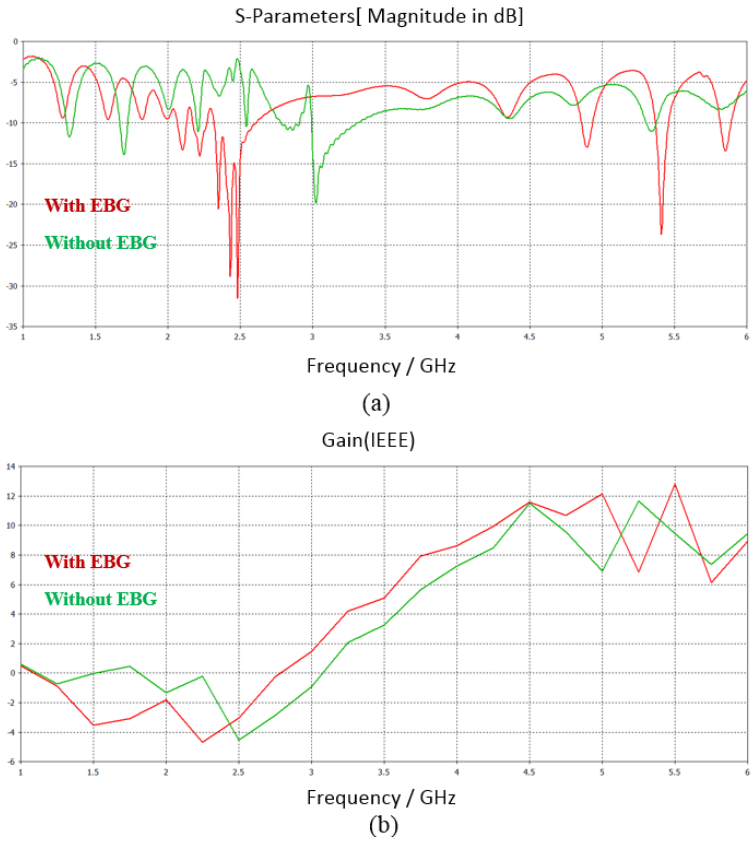

Fig. 9. EBG defects parametric study (a) S_{11} (b) gain.

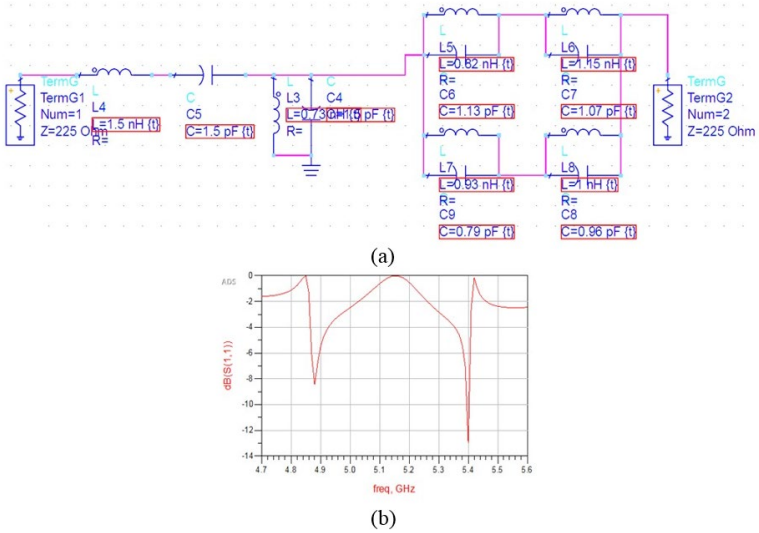

Fig. 10. (a) ADS equivalent circuit (b) S_{11}.

4. Frequency Reconfigurable Antenna Simulation Study

The metamaterials usually consist of resonant structures that exhibit different behaviours depending on the resonant frequency [32], which is considered a disadvantage because most practical wireless applications must have fixed and unchanging resonance frequencies. Therefore, to have an antenna capable of working in various wireless applications and with different frequencies, the antenna must be reconfigurable [33], as the operating frequency can be controlled by changing the applied voltage and thus obtaining a multi-characteristic antenna. Here, the metasurface is created through periodically arranged a T-symmetric CRLH-MTM. A gap is inserted in each inductor, and one PIN diode is used in each gap for frequency reconfigurability, see Fig. 11.

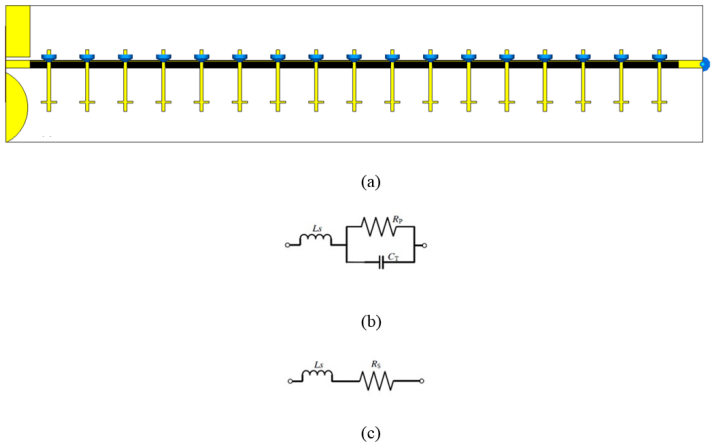

Fig. 11. Antenna structure: (a) 3D antenna structure, (b) Equivalent circuits of the PIN diode OFF-state, and (c) ON-state.

By changing the state of the PIN diode, multiple bands can be obtained with different resonant frequencies, whereby the operating frequency can be adjusted according to the input sequence of the PIN diode. Table 1 represents the input sequence of the PIN diode, its corresponding operating frequency, and the number of bands formed.

Table 1. Frequency reconfigurable study.

Input sequence	Number of bands	Resonance frequency in GHz
00000000000000000	3	4.8, 5.4, 5.8
11111111000000000	4	5.2, 4.2, 4.7, 5.6
11000000000000000	4	5.3, 4.8, 5.8, 4.3
11100000000000000	4	5.2, 4.3, 4.9, 5.7
11111111111111111	5	4.2, 4.6 , 5, 5.5, 5.8
11100111011100111	5	4.2, 4.7 ,5.1, 5.6, 5.9

For the previous cases, gain and S_{11} are calculated. The array gain reached a maximum value when the PIN was turned off at 5.5 GHz with a gain of 12.4 dBi (refer to Fig. 12).

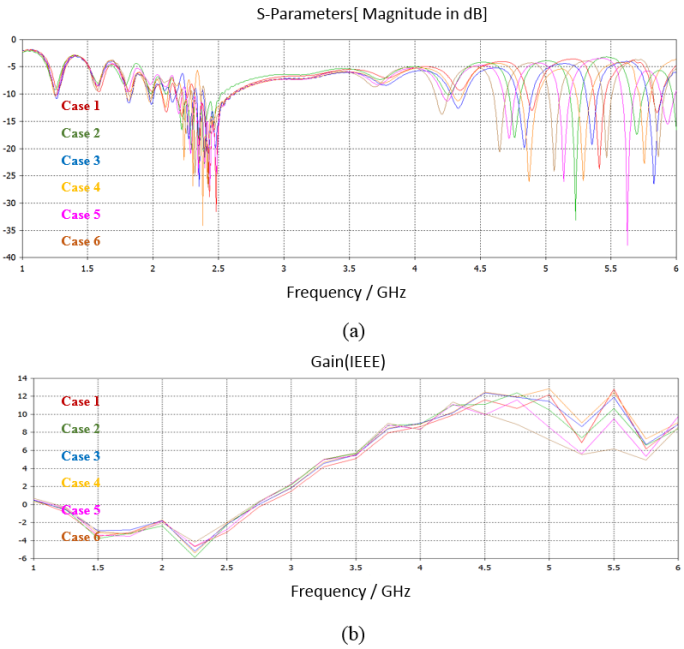

Fig. 12. Frequency reconfigurable: (a) S_{11} (b) gain.

5. Comparison with Latest Research

In this section, a comparison with the field of interest is summarized and presented in Table 2; It is good to mention that (F) refers to the frequency, (Pa) refers to the pattern, and (Po) refers to polarization. It is clear from the comparison that the proposed antenna provides the highest gain with excellent impedance matching at the frequency of operation, In addition to the possibility of reconfiguration and

gains control. Such achievement nominates the antenna for applications of frequency reconfiguration and gain control for sub 6 5G wireless networks.

Table 2. Comparison with the field of interest.

Ref.	frequency GHz	Reconfig ure	Technique	gain dBi	PIN .NO	Design type / size mm²
[13]	3.1, 4.1, 3.8 , 2.45, 7.8 , 9.5	F/ pa	Hexagon patch-CPW	4.24	2	Single / 30 × 20
[14]	2.4 &5.8	F	slots	4		Single / 30*35
[15]	2.4 & 5.8	pa	EBG	6.6	14	Single / 113*113
[16]	2.6 , 3.5 , 4.2 , 4.5 , and 5, 5.5	F/ pa	parasitic patches.	3.8	8	Single / 31 × 27
[17]	4.66,5.2, 5.3, 5.8	F	V-Shaped microstrip	6	2	Single / 16 × 16
[18]	5.8	pa	slots	4.33	2	Single
[19]	5.8	Po	truncated patch	11.9	16	Array/ 70×70
[34]	5.8	Po	superstrate/ array of patches	3.7	2	Array/ 84*50
[35]	4.8 to 6	Po	truncated patch/ metasurface	7.3	2	Single / 48*48
[36]	6.2–6.8, 8.5–9.2 5.9–6.5	F	Half-mode CRLH	5.21	1	Single / 22×27
[37]	3.5, 5.5	__	CRLH	4.1	____	Single / 24×17
[38]	2.4/5.2,	F/Po	CRLH/ SRR	3	2	Single / 40×40
[39]	5.0–5.9	Pa	CRLH	10.4	____	Single / 64×64
This work	4.2-4.3, 4.6- 4.9 ,5 -5.9	F	CRLH/ Minkowski – SIR	12.4	17	1D-Array / 40*240

6. Conclusion

The design of fractal-MTM -via free antenna is proposed by loading Minkowski -SIR curve on CRLH-MTM; the structure is composed of a 17-unit cell of CRLH coupled to an EBG inclusion etched on the back surface of Taconic FR-4 substrate. The antenna radiation performance is calculated in terms of gain and S_{11}.

In addition, the equivalent circuit model using ADS software was calculated and compared to CST results; a good agreement is found between the two results. The proposed design is controlled using a 17 PIN diode to change the antenna's characteristics and its resonance frequency according to the bias voltage.

Six cases are selected among 2^{17} cases to show the antenna ability for reconfiguration and gain control. The antenna covers the bands (4.2 GHz -4.3 GHz), (4.6 GHz -4.9 GHz), and (5 GHz -5.9 GHz) with good gain among the operated bands. Finally, At off state, Minkowski –SIR antenna has dual-band at 4.89 GHz and 5.4 GHz with gain equal to 12.4 dBi and 10.8 dBi, respectively. The proposed design can be used in Wi-Max, Wi-Fi, Satellite communication downlink, and 5G sub-6-GHz and radar applications.

Nomenclatures

C_{IDC}	Inter-digital capacitor
L_{Ts}	T-stub inductor

Abbreviations

CRLH	Composite Right/Left Hand
EBG	Electromagnetic Band Gap
MTM	Metamaterial
PEC	Perfect Electric Conductor
SIR	Stepped Impedance Resonator

References

1. Ali, J.K.; Abdul-Baki, E.M.; and Hammed, M.H. (2010). A multiband fractal dipole antenna for wireless communication applications. *Engineering & Technology Journal*, 28(10), 2043-2053.
2. Mustafa, O.I.; Ismail, M.M.; and Bashar, B.S. (2021). Parasitic slotted patch antenna for dual-band operation over S-band. *Proceedings of the* 2021 *IEEE* 8*th International Conference on Problems of Infocommunications*, *Science and Technology* (*PIC S&T*), Kharkiv, Ukraine, 564-568.
3. Zaidan, A.A.; Zaidan, B.B.; Qahtan, M.Y.; Albahri, O.S.; Albahri, A.S.; Alaa, M.; Jumaah, F.M.; Talal, M.; Tan, K.L.; Shir, W.L.; and Lim, C.K.(2018). A survey on communication components for IoT-based technologies in smart homes. *Telecommunication Systems*, 69(1), 1-25.
4. Zhang, K.; Soh, P.J.; and Yan, S. (2020). Meta-wearable antennas - A review of metamaterial based antennas in wireless body area networks. *Materials*, 14(1):149, 1-20.
5. Ameen, M.; and Chaudhary, R.K. (2020). Dual-layer and dual-polarized metamaterial inspired antenna using circular-complementary split ring resonator mushroom and metasurface for wireless applications. *AEU - International Journal of Electronics and Communications*, 113, 152977.
6. Wang, Z.; Ning, Y.; and Dong, Y. (2021). Hybrid metamaterial-TL based, low-profile, dual-polarized omnidirectional antenna for 5G indoor application. *IEEE Transactions on Antennas and Propagation*, 70(4), 2561-2570.
7. Ameen, M.; Mishra, A.; and Chaudhary, R.K. (2021). Dual-band CRLH-TL inspired antenna loaded with metasurface for airborne applications. *Microwave and Optical Technology Letters*, 63(4), 1249-1256.
8. Liu, L.; and Shi, X. (2022). Broadband circularly polarized CPW-fed monopole antenna with a via-free CRLH-TL unit cell. *International Journal of Antennas and Propagation*, Volume 2022, Article ID 7168470.
9. Rasool, J.M. (2010). MIMO antenna system using orthogonally polarized ultra wide band antennas with metamaterial. *Engineering and Technology Journal*, 28(24), 6845-6853.
10. Das, G.K.; Basu, S.; Mandal, B.; Mitra, D.; Augustine, R.; and Mitra, M. (2020). Gain-enhancement technique for wearable patch antenna using grounded metamaterial. *IET Microwaves*, *Antennas & Propagation*, 14(15), 2045-2052.

11. Mohamadwasel, N.B.; and Abdala, M.A. (2020). Design of WiMAX network for Istanbul Universities With OPNET. *Informatica on Applied Machines Electrical Electronics Computer Science and Communication Systems*, 1(1), 1-9.
12. Ameen, M.; and Chaudhary, R.K. (2020). Electrically small circularly polarized antenna using vialess CRLH-TL and fractals for L-band mobile satellite applications. *Microwave and Optical Technology Letters*, 62(4), 1686-1696.
13. Ullah, S.; Elfergani, I.; Ahmad, I.; Din, I.U.; Ullah, S.; Rehman Khan, W.U.; and Rodriguez, J. (2022). A compact frequency and radiation reconfigurable antenna for 5G and multistandard Sub-6 GHz wireless applications. *Wireless Communications and Mobile Computing*, Volume 2022, Article ID 4658082, 1-12.
14. Al-Saeedi, M.M.; Hashim, A.A.; Al-Bayati, O.H.; Rasheed, A.S.; and Finjan, R.H. (2021). Design of dual band slotted reconfigurable antenna using electronic switching circuit. *Indonesian Journal of Electrical Engineering and Computer Science*, 24(1), 386-393.
15. Ismail, M.F.; Rahim, M.K.A.; Hamid, M.R.; Majid, H.A.; Omar, A.H.; Nur, L.O.; and Nugroho, B.S. (2021). Dual-band pattern reconfigurable antenna using electromagnetic band-gap structure. *AEU - International Journal of Electronics and Communications*, 130, 153571.
16. Ahmad, I.; Dildar, H.; Khan, W.U.R.; Shah, S.A.A.; Ullah, S.; Ullah, S.; and Vasudevan, K. (2021). Design and experimental analysis of multiband compound reconfigurable 5G antenna for Sub-6 GHz wireless applications. *Wireless Communications and Mobile Computing*, Volume 2021, Article ID 5588105, 1-14.
17. Reji, V.; and Manimegalai, C.T. (2021). V-shaped long wire frequency reconfigurable antenna for WLAN and ISM band applications. *AEU - International Journal of Electronics and Communications*, 140, 153937.
18. Prakash, T.; Chaudhary, R.K.; and Gangwar, R.K. (2021). Quad-beam octa cross-slotted pattern reconfigurable antenna for 5.8 GHz band application. *Proceedings of the* 2020 50*th European Microwave Conference* (*EuMC*), Utrecht, Netherlands,710-713.
19. Anantha, B.; Merugu, L.; and Rao, P.V.D.S. (2021). Polarization reconfigurable corner truncated square microstrip array antenna. *IETE Journal of Research*, 67(4), 491-498.
20. Alibakhshikenari, M.; Virdee, B.S.; Khalily, M.; Shukla, P.; See, CH; Abd-Alhameed, R.; Falcone, F.; and Limiti, E. (2019). Beam-scanning leaky-wave antenna based on CRLH-metamaterial for millimetre-wave applications. *IET Microwaves*, *Antennas & Propagation*, 13(8), 1129-1133.
21. Alibakhshikenari, M.; Virdee, B.S.; Althuwayb, A.A.; Azpilicueta, L.; Parchin, NO; See, CH; and Limiti, E. (2021). Bandwidth and gain enhancement of composite right left handed metamaterial transmission line planar antenna employing a non foster impedance matching circuit board. *Scientific Reports*, 11, Article number: 7472, 1-11.
22. Meinzer, N.; Barnes, W.L.; and Hooper, I.R. (2014). Plasmonic meta-atoms and metasurfaces. *Nature Photonics*, 8(12), 889-898.

23. Ntawangaheza, J.d.D.; Sun, L.; Li, Y.; and Xie, Z. (2020). Improving bandwidth, gain and aperture efficiency of patch antenna using hybrid AMC ground plane. *Progress in Electromagnetics Research C*, 103, 71-82.
24. Vassos, E.; Churm, J.; and Feresidis, A. (2020). Ultra-low-loss tunable piezoelectric-actuated metasurfaces achieving 360° or 180° dynamic phase shift at millimeter-waves. *Scientific Reports*, 10, Article number: 15679, 1-10.
25. Alibakhshikenari, M.; Virdee, B.S.; Azpilicueta, L.; Naser-Moghadasi, M.; Akinsolu, M.O.; See, CH; and Limiti. (2020). A comprehensive survey of "metamaterial transmission-line based antennas: Design, challenges, and applications. *IEEE Access*, 8, 144778-144808.
26. Melouki, N.; Hocini, A.; and Denidni, T.A. (2021). Performance enhancement of a compact patch antenna using an optimized EBG structure. *Chinese Journal of Physics*, 69, 219-229.
27. Ismail, M.M.; Elwi, T.A.; and Salim, A. (2022). A miniaturized printed circuit crlh antenna-based Hilbert metamaterial array. *Journal of Communications Software and Systems*, 18(3), 236-243.
28. Bhavarthe, P.P.; Rathod, SS; and Reddy, K.T. (2017). A compact two via slot-type electromagnetic bandgap structure. *IEEE Microwave and Wireless Components Letters*, 27(5), 446-448.
29. Máximo-Gutiérrez, C.; Hinojosa, J.; Martínez-Viviente, F.L.; and Alvarez-Melcon, A. (2020). Design of high-performance microstrip and coplanar low-pass filters based on electromagnetic bandgap (EBG) structures. *AEU - International Journal of Electronics and Communications*, 123, 153311.
30. CST program (2022), Retrieved June 18, 2022, from https://www.3ds.com/products-services/simulia/products/cst-studio-suite/#:~:text=CST%20Studio%20Suite%C2%AE%20is,(EM)%20components%20and%20systems.
31. Ziboon, H.T.; and Ali, J.K. (2017). Compact quad-band BPF design with fractal stepped-impedance ring resonator. *ARPN Journal of Engineering and Applied Sciences*, 12(24), 7352-7363.
32. Ahmed, H.S.; Ali, J.K.; and Salim, A.J. (2017). Design of fractal-based bandstop filter for microwave radiation leakage reduction. *Engineering and Technology Journal*, 35(1A),16-23.
33. Awan, W.A.; Naqvi, S.I.; Ali, W.A.E.; Hussain, N.; Iqbal, A.; Tran, H.H.; Alibakhshikenari, M.; and Limiti, E. (2021). Design and realization of a frequency reconfigurable antenna with wide, dual, and single-band operations for compact sized wireless applications. *Electronics*, 10(11), 1321.
34. Roseli, W.I.; Ali, M.T.; Abd Rahman, N.H.; Aris, M.A.; and Yon, H. (2019). Performance enhancement of polarization reconfigurable antenna for wireless communication applications. *Proceedings of the* 2019 *International Symposium on Antennas and Propagation* (*ISAP*), Xi'an, China, 1-4.
35. Tran, H.H.; Bui, C.D.; Nguyen-Trong, N.; and Nguyen, T.K. (2021). A wideband non-uniform metasurface-based circularly polarized reconfigurable antenna. *IEEE Access*, 9, 42325-42332.
36. Gunamony, S.L.; Bala, G.J.; Raj, S.M.G.; and Pratap, C.B. (2021). Asymmetric coplanar strip-fed electrically small reconfigurable 5G mid-band antenna. *International Journal of Communication Systems*, 34(15), e4935 1-11.

37. Ashish, J.; and Rao, A.P. (2022). A dual band CRLH metamaterial-inspired planar antenna for wireless applications. *Radioengineering*, 31(1),15-22.
38. Ghosh, K.; and Das, S. (2022). CRLH-TL based reconfigurable antennas with multiple parameter reconfigurability. I*EEE Transactions on Antennas and Propagation*, 70(7), 5892-5896.
39. Yan, S.; Zheng, Y.; Wang, B.; Zhang, J.; and Vandenbosch, G.A.E. (2021). A low-profile wideband microstrip antenna with pattern diversity based on composite right/left-handed transmission lines. *IEEE Antennas and Wireless Propagation Letters*, 20(8), 1478-1482.